Modelling of the hydro-acoustic signal and tsunami wave generated by sea floor motion including a porous seabed

Francesco Chierici

Istituto di Radioastronomia, Istituto Nazionale di Astrofisica, sezione Bologna, via Gobetti, 101 - 40129 Bologna, Italy

Luca Pignagnoli

Istituto di Scienze Marine, Consiglio Nazionale delle Ricerca, sezione Bologna, via Gobetti, 101 - 40129 Bologna, Italy

Davide Embriaco

Istituto Nazionale di Geofisica e Vulcanologia, sezione Roma 2, via Pezzino Basso, 2 - 19025 Portovenere (SP), Italy

F. Chierici, IRA-INAF (chierici@ira.inaf.it)

Abstract Within the framework of a 2-D compressible tsunami generation model with a flat porous seabed, acoustic waves are generated and travel outwards from the source area.

The effects of the porous seabed during tsunami generation and propagation processes include wave amplitude attenuation and low pass filtering of both the hydro-acoustic signal and tsunami wave. The period of the acoustic wave generated by the seafloor motion depends on water depth over the source area and is given by four times the period

of time required for sound to travel from the sea bed to the surface: these waves carry information about seafloor motion.

The semi-analytical solution of the 2-D compressible water layer model overlying a porous seabed is presented and discussed.

Furthermore, to include the effects generated by the coupling between compressible porous sedimentary and water layers, a simplified two layer model with the sediment modelled as a compressible viscous fluid is presented.

1. Introduction

Tsunami waves, which travel long distances at speeds depending on water depth, can be extremely dangerous and destructive, as shown by the recent disastrous Sumatra earthquake (e.g. *Lomnitz and Nilsen-Hofseth*, [2005], *Merrifield et al.,* [2005]). Tsunamis can be generated by different mechanisms, such as shallow submarine earthquakes, sub-aerial and submarine landslides or volcanic eruptions and consequent submarine landslides [*Synolakis et al.,* 2002; *Tinti et al.,* 2004], meteoric impacts or meteorological tsunami. The most common and effective mechanism derives from earthquakes, as reported by historical sources (e.g. *Boschi et al.,* [1997]; *Tinti et al.,* [2004], NGDC Tsunami Catalog, *Bernard and Robinson*, [2009]).

From the 1980s onwards, many different theoretical approaches, both analytical (e.g. *Ward,* [1980]; *Comer,* [1984]; *Okal,* [1988]; *Panza et al.,* [2000]) and numerical (e.g. , *Kowalik et al.,* [2005]), have been developed to model tsunami generation. Most of

these studies take into account a wide variety of physical characteristics within the framework of incompressible fluid theory with few exceptions (e.g., *Nosov*, [1999]; *Ohmachi et al.,* [2001]). These theoretical approaches are mainly based on an absolutely rigid bed, or alternatively on an elastic half-space, coupled with an incompressible water layer in a spherical domain [*Ward,* 1980; 1981; 1982] or in a plane domain [*Comer,* 1984] or coupled with a stratified incompressible fluid [*Panza et al.,* 2000]. In spite of the great scientific and technological effort made to deal with the tsunami hazard over the past few years and the numerous studies performed on tsunamigenic sources [*Ma et al.,* 1997; *Synolakis et al.,* 1997; *Zitellini et al.,* 1999; *Baptista et al.,* 2003], propagation and the flooding caused by tsunami waves [*Synolakis,* 1995], the details of tsunami generation processes are still poorly understood, mainly because of the scarcity of direct measurements in tsunami generation areas. Recently, some authors have accounted for the significant role played by water compressibility in tsunami generation, showing that this compressibility is significant in tsunami generation but not in their propagation [*Nosov,* 1999; *Nosov and Skachko*, 2002; *Nosov et al.,* 2007; *Nosov and Kolesov ,* 2007].

The general contribution of compressibility in tsunami evolution has been presented by *Miyoshi* [1954], *Sells* [1965] and *Kajiura* [1970]. The assumption of the compressibility of the water layer allows the sound waves, which are pressure waves, to form and propagate into the water layer [*Gisler*, 2008].

Summarizing the modelling of tsunami generation is still in its infancy compared to propagation modelling. Compressibility is likely to be relevant in all circumstances where rock motion is coupled to water motion, and there are very few models which properly account for this imperfect coupling and the generation of acoustic waves,

turbulence, and even shock waves in extreme cases. Compressibility may also be of significant importance in calculating the impact of tsunami waves on structures.

The low-frequency acoustic waves generated throughout the entire water column by seismic seafloor motion should not be confused with the high-frequency acoustic waves from earthquakes (T-waves) which are channeled into an underwater wave guide, known as SOFAR. *Okal et al*. [2003] proposed a new approach to tsunami early warning based on this particular kind of acoustic wave: the presence of a potential tsunami would be signalled by an energy deficiency in the frequency band of the T-waves produced by the earthquake.

The first convincing experimental proof of the existence of low-frequency elastic waves generated throughout the entire water column by the seabed motion, with frequency inversely proportional to the water depth was obtained during the Tokachi-Oki 2003 tsunami event, when the real-time JAMSTEC observatory detected the acoustic pressure signal, with a 0.15 Hz frequency peak, generated by the seafloor motion caused by the earthquake [*Nosov et al.,* 2007]. The two pressure sensors were located in the epicenter area, allowing direct measurement of water pressure variation during the earthquake. The spectral analysis of the pressure signal clearly shows the low-frequency elastic oscillation of the water column as expected and predicted by the compressible fluid formulation and also shows other frequency components [*Nosov et al.,* 2007]. As expected from the theory, the elastic oscillation carries information on the water-column height above the source (with a maximum depth of about 7500m in the Tokachi-Oki area and about 2200-2300m at the pressure sensor locations).

However, the 3-D compressible numerical model used by *Nosov and Kolesov*, [2007], fails to reproduce the order of magnitude of the acoustic band power spectrum generated during the Tokachi-Oki 2003 event. Moreover it does not match the lower frequency value, measured by the pressure sensors, of the expected peak due to the water layer oscillation. To address these critical points in *Nosov and Kolesov* [2007], the introduction of a sedimentary porous layer, modelled using the Darcy equation, beneath the compressible water column should be considered. In fact the sedimentary layer causes the damping of water and hydro-acoustic waves generated by sea floor motion, lowering the whole energy spectrum, with the compressibility of the porous layer "shifting" the expected frequency peak toward a lower value.

We present here a model which, by taking into account water compressibility and porous seabed, highlights some important characteristics of tsunami generation processes which can enhance present tsunami warning capabilities and increase the understanding of the source ground motion.

2. Model

We have developed a new 2-D model with a compressible water column overlying a porous layer, which is solved semi-analytically (see Appendix A) by merging the methods used in *Nosov and Sammer ,*[1998], *Nosov,* [1999] and *Nosov,* [2000] and in *Gu and Wang,* [1991] and *Habel and Bagtzoglou,* [2005]. We assumed the approximation of small-amplitude waves that allows us to simplify the model to a linear problem. The linearity of the equations allows the composition of simple motions (i.e., permanent

displacements and elastic sinusoidal displacements) to model much more complicated motion with various source parameters, initial polarity, amplitudes, phases, durations (see subsection 4.0 in Discussion).

For the sake of simplicity and brevity we focus only on some aspects of the simulations of tsunami and hydro-acoustic signal generation, which are better illustrated by showing the solution in the water layer and for permanent displacement. The Navier-Stokes equation is the governing equation in the water layer:

$$\begin{cases} \dfrac{\partial \rho}{\partial t} + \nabla \cdot \left(\rho \vec{\mathrm{U}} \right) = 0 \\ \dfrac{\partial \vec{\mathrm{U}}}{\partial t} + \underline{\vec{\mathrm{U}} \cdot \nabla \vec{\mathrm{U}}} = -\dfrac{1}{\rho} \nabla P - \vec{\mathrm{g}} + \underline{\nu \nabla^2 \vec{\mathrm{U}}} + \underline{\nu_2 \nabla (\nabla \cdot \vec{\mathrm{U}})} \end{cases} \qquad (1)$$

where ρ is the water density, U the fluid velocity, P the pressure, v the kinematic viscosity, v_2 the second viscosity and g the gravitational acceleration.

We have introduced some simplifying assumptions to solve the model. In particular, we use the small amplitude wave approximation, i.e., the wave amplitude is small with respect to its wavelength, which also applies to huge tsunami waves in the open ocean, and the non-viscous fluid approximation in the water layer (viscosity is not significant on typical tsunami scales). As a consequence the underlined quantities in equation (1) become negligible.

Assuming irrotational flow in the water column, the fluid velocity field U is described by the potential φ(x,z,t):

$$A / \lambda << 1 \quad (2)$$

$$\vec{U} = \nabla \varphi \quad (3)$$

where A is the wave amplitude and λ is the wavelength. All departures from the assumption of fluid at rest with uniform density ρ_0 are regarded as small quantities. We assume P = P(ρ) that is linearized using a Taylor expansion (see *Lamb,* [1932]; *Lighthill,* [1993]), so the equation of state reduces to:

$$P = P(\rho_0) + (\rho - \rho_0)\frac{\partial P}{\partial \rho}(\rho_0) + \ldots = P(\rho_0) + (\rho - \rho_0)c^2 + \ldots \quad (4)$$

where c is the sound speed in water (about 1500 m/sec, depending on sea water temperature and salinity), here considered as constant due to the hypothesis of small fluctuations.

Applying assumptions (2), (3) and (4) to equations (1) we obtain:

$$\nabla^2\varphi=\frac{1}{c^2}\frac{\partial^2\varphi}{\partial t^2}(5)$$

$$P=-\rho\frac{\partial\varphi}{\partial t}-\rho gz(6)$$

z is the vertical axis positive in the upward direction.

In the porous layer we use the Darcy equation:

$$\begin{cases}\nabla\cdot\vec{Q}=0\\ \nabla P_s=\dfrac{\mu}{K_p}\vec{Q}+\dfrac{\rho}{n}\dfrac{\partial\vec{Q}}{\partial t}\end{cases}(7)$$

where $\boldsymbol{Q}$=(Q_x, Q_z) is the discharge velocity, P_s the pore pressure, K_p and n the intrinsic permeability and volumetric porosity, respectively, μ and ρ are the dynamic viscosity and density of the fluid. This approach differs from the visco-elastic model proposed by Biot for porous media [*Biot*, 1962], because we do not consider the elastic deformation of the solid matrix.

The boundary conditions at the free surface (z=0) are

$$\frac{\partial \varphi}{\partial t} = -g\xi\Big|_{z=0} \quad (8)$$

$$\frac{\partial \xi}{\partial t} = \frac{\partial \varphi}{\partial z}\Big|_{z=0} \quad (9)$$

representing the dynamic and kinematic conditions, respectively, where ξ is the free surface perturbation. The boundary conditions at the water-sediment interface (z =-h) are

$$\rho \frac{\partial \varphi}{\partial t} = P_s\Big|_{z=-h} \quad (10)$$

$$\frac{\partial \varphi}{\partial z} = Q_z\Big|_{z=-h} \quad (11)$$

representing the continuity of the stress field and the vertical component of the fluid velocity, respectively, where *h* is the water column height.

Assuming the non-permeability of the "bottom", defined as the surface underlying the porous sedimentary layer, the boundary condition at the base of the sedimentary layer is given by

$$Q_z = \left.\frac{\partial \eta}{\partial t}\right|_{z=-h-h_s} \quad (12)$$

where $\eta(x,t)$ is the bottom motion. The small-amplitude approximation, $\eta/h<<1$, must be satisfied; h_s is the sediment thickness. In figure 1 some examples of seafloor motion used below are displayed. The discontinuous derivatives implied by the cusp points in the left panel of figure 1 are quite unphysical, but they do not affect the physical essence of the main results presented here.

Equations (5) and (7) are solved to obtain the potential field and pressure in the porous layer by taking a Fourier transform with respect to x and Laplace transform with respect to the time t:

$$\varphi(x,z,t) = \frac{1}{4\pi^2 i}\int_{s-i\infty}^{s+i\infty} d\omega \int_{-\infty}^{+\infty} dk\; e^{\omega t - ikx} \times [A(k,\omega)\sinh(-\alpha\, z) + B(k,\omega)\cosh(-\alpha\, z)] \quad (13)$$

$$P_s(x,z,t) = \frac{1}{4\pi^2 i}\int_{s-i\infty}^{s+i\infty} d\omega \int_{-\infty}^{+\infty} dk\; e^{\omega t - ikx} \times [C(k,\omega)\sinh(-k\, z) + D(k,\omega)\cosh(-k\, z)] \quad (14)$$

from which the desired quantities can be computed using (3), (6) and (8). The A, B, C, D and α expressions are given in Appendix A.

3. Results

The model allows the study of signal amplitude and shape in the water layer at various distances and depths and for different bottom motions. In this paper we have presented a simple kind of motion, i.e., the piston-like motion caused by a seabed displacement of fixed length 2a, which rises at constant velocity v_B , reaching the final elevation η_0 after a time τ (permanent displacement). Solutions can be easily obtained for more complicated motion, due to linearity (see subsection 4.0 in Discussion). The seafloor motion is modelled using the dynamic approach proposed by *Nosov*, [1999]. The traditional static approach consisting of an instantaneous translation of the seafloor deformation to the free surface, computed by using, for instance, the *Okada*, [1985] model, neglects the effect of the moving bed velocity in tsunami generation (see *Dutykh*, [2006] for a comparison between the two approaches).

As a consequence of model linearity, it can also be shown that all the output parameters (i.e., sea level displacement ξ, pressure P, etc.) are proportional to seafloor motion amplitude η_0. The indicative value of η_0=1m for the amplitude of the vertical displacement has been used in the following.

The model presented here reduces to Nosov's compressible model [Nosov, 1999], within the limit of null-sediment thickness ($h_s \rightarrow 0$). The main effect of the porous layer is the attenuation of the signal amplitude, during the generation and propagation phases, and also a high frequency smoothing (Figure 2, boxes a, c and d). The porous layer causes an attenuation of the power spectrum amplitude with respect to the compressible case without sediment (Figure 2c), which is so relevant for higher frequencies as to become a real cut-off effect (Figure 2d). The tsunami wave amplitude is also influenced, during generation and propagation, by the presence of a porous layer causing a reduction of the wave amplitude compared to the compressible case without porous sediment (Figure 2a and b).

The assumption of compressibility in the water column leads naturally to the generation of acoustic waves in the water layer in addition to tsunami formation [*Nosov and Skachko,* 2001; *Gisler,* 2008]. The model allows the study of the effects of wide sources (much larger than water depth) on the tsunami generation process; as a consequence of the model, acoustic wave generation continues after the sea-floor motion stops, due to the coherent elastic oscillation of a large portion of the displaced water layer being subjected to the gravitational restoring force.

The propagation of hydro-acoustic waves outwards from the generation area, with frequencies lower than the proper frequency of the water layer is affected by the porous sedimentary layer: the resulting behavior, in fact, is different from that expected in the case of an elastic basement, where there is a propagation cut-off, due to the waveguide formed by the water free surface and elastic sea floor [*Tolstoy,* 1963]. As shown in [*Naoi et al.* 2006], if the effect of a sediment layer is considered, then the attenuation of the low

frequency acoustic waves, propagating toward shallower water, is not as strong as in the case of an elastic sea floor, due to the coupling between the water layer and the sediment.

Below we show results in which tsunami formation and the hydro-acoustic signal in the water layer are obtained by taking into account a porous sediment and water column compressibility.

In Figure 3, boxes a and b, the water surface disturbance for observation points at different distances from the source is shown (the virtual pressure sensor is located at the water surface). Figure 3, boxes c and d, show the same simulation, with the virtual pressure sensor located at a depth of 1500m; here the vertical axis unit is given in hPa, roughly corresponding to 1 cm of equivalent water column height. The details of the source length and motion are given in the figure caption together with the other parameters. Figure 3 clearly shows the tsunami and the acoustic signal with its modulation. Within the framework of the model the signal amplitude decreases with the distance as $x^{-1/2}$, showing low attenuation at a long distance from the source. The signal vibrates at frequencies $\nu_l = c(2l+1)/4h$, where h is the water depth and l=0, 1, 2 ..[*Nosov,*1999]. The acoustic signal reaches the observing points at time $t_s=x_s/c$, where x_s is the distance from the source, well preceding the arrival of the tsunami wave, which travels at a lower speed $\nu_T = (gh)^{1/2}$. There is a difference in shape between the acoustic signal modulation at the water surface and at depth, completely described by the function $f_p\ (\omega, k, z)$ in the (ω, k) domain (see Appendix A), which acts as a transfer function between the signal at depth and at the free surface.

The amplitude modulation shown by the acoustic waves presents an interesting feature from which, at least within the framework of the model, information on source motion and its geometry can be extracted.

Figures 4 and 5 show the various acoustic modulations produced by sources of different lengths, moving at different velocities and their comparison. We have analyzed the envelopes of the acoustic signals, finding unexpected correlations among source length, envelope mean slopes, and the number of envelope pulses over a given time interval (Figure 4), and between the mean slopes and the source velocities (Figure 5). The mean slope has been defined as the difference between the relative maximum and minimum of the single pulse, divided by the pulse semi-length (i.e., it is the incremental ratio: the tangent of the angle formed with the horizontal axis by the chord connecting the pulse maximum and minimum).

The envelopes can be obtained by applying a demodulation technique to the signals, for instance, a Hilbert transform or the "square and low pass".

In particular, Figure 4 shows that the number of pulses is proportional to the source length: increasing the length of the source, the number of pulses within a time-interval increases according to the ratio between the source lengths. The mean slopes of the pulses also scales proportionally with the source lengths.

Figure 5 shows the modulation caused by the same seafloor motion as in Figure 4, but with different velocities v_B of the source, here chosen with a length of 2a=30 km. Although of different amplitudes, the modulations appear to be quite similar. The mean slope of the pulses scales with the same ratio of the various velocities.

The mean slope of the pulses varies with the energy released by the bottom motion into the water layer. The expression of the energy transmitted to the water layer by the sea-floor motion, within the framework of a compressible model, is given by $W=\rho c V^2 S\tau$ where S is the source area, V the sea bottom velocity and τ the duration of the motion [*Nosov* ,1999; *Nosov and Kolesov,* 2007]. The quantities which linearly vary the energy are the same that linearly vary the mean slopes of pulses and their number over a given time interval (rewritten as $W=\rho c V L \eta_0$, having substituted $V=\eta_0/\tau$ and S with the source length because of the 2-D model). Hence the mean slope can be effectively considered as an indicator of the energy released by the bottom motion into the water layer.

Thus, by using a semi-empirical approach towards data interpretation, we have shown that, at least within the framework of the model, the information about the source length, the ground motion velocity and amplitude, and the water depth at the source location can be extracted from the arrival of the very first pulse of the acoustic signal. In principle, if hydro-acoustic waves generated by bed motion are detected, this information could also be extracted from a real signal.

Particular cases occur when the period of the bottom motion is similar to the fundamental one of the water column oscillation and when the length of the source is smaller than the water depth.

When the frequency of ground motion and the fundamental frequency of oscillation v_0 of the water column present similar or commensurable values (i.e., kv_0, k=1,2,..), then an "interference" occurs between these two frequencies. As shown in

Figures 6, in this "interference" situation the hydro-acoustic signal shape and modulation are quite different from those produced by ground motions with periods far from the fundamental period $T=1/\nu_0$. In this figure the proper frequency of the water layer is 0.25 Hz and we use this same frequency and its harmonics for the bed motion (see Figure 6 caption for details of the simulation). It can be seen that not only the shape of the modulation in the "interference" case is quite different from the “non-interference” one (see Figures 4(a), (b) and 5(a), (b), (c) for comparison) but the amplitude of the "interference" signal is much smaller. The "interference" modulation scales monotonically with the seafloor velocity. The envelopes of Figure 6 again show a linear relationship between mean slopes and bottom velocities (Figure 6c) with a correlation coefficient r^2=0,9987 (Figure 6d). After the first train of pulses, which scales proportionally with the velocities, before the tsunami arrives, the modulations turn into tails where the magnitude of the signals is almost the same for any "interference frequency": differences are of the order of 10^{-3} times the signal amplitude values. The very first part of the demodulation must be ignored in this particular case because the low pass filter demodulation technique fails to closely follow the first high frequency pulses, due to the filter parameter settings. The interference caused by a seafloor motion with a period equal to that of the seawater-layer fundamental oscillation does not erase the source parameter information carried by the acoustic signal and, at least within the framework of this model, this information can be retrieved. This result also remains valid for much more complicated motions (see subsection 4.0 in Discussion). On the contrary, the tsunami wave amplitude is not affected by this kind of interference (see Figure 7).

In Figure 8 the power spectra of "interference" and "non-interference" modulations are shown. Both spectra are peaked at the fundamental frequency of the water layer. Odd harmonics are also present. The "interference" spectrum is characterized by a lower amplitude of the peaks, but a much more broadly distributed power.

At the limit of source lengths smaller than the water depth (for instance, modelling a point source, $a/h<1$), corresponding to the second particular case mentioned above, the hydro-acoustic signal shows no modulation (Figure 9), with the consequent loss of information about the source parameters, as obtained numerically by *Gisler* [2008].

4. Discussion

Some results of a 2-D semi-analytical model for tsunami generation have been presented for the case of "piston-like" motion with residual permanent displacement, taking into account water compressibility and seabed porosity. In Section 4.0 below we show that much more complicated sea-bottom motions can be obtained by combining the piston-like motion and the time-shift operator. Appendix A shows that the acoustic modulation obtained at depth can be always related to an equivalent "representation of acoustic modulation" at the free surface. Appendix B (section Tokachi-Oki mismatch) proposes a simplified model, to take into account compressibility, both in water and the sedimentary layer, to address a critical point presented in *Nosov and Kolesov* [2007].

4.0 Relationship between permanent displacement and more complicated seafloor motions.

Notwithstanding the fact that the above results were obtained for only permanent displacement, they remain valid for much more complicated bed motions. As mentioned above, these various kinds of motion can be constructed by starting from the permanent displacement. Due to the linearity of the model a similar relationship can also be obtained between the corresponding solutions. For example the simplest elastic seafloor motion (rise and fall, second row of figure 1) identified by $\eta_e(t)$ can be constructed as:

$$\eta_e = (1 - \mathbf{T}_\tau)\eta_p \qquad (15)$$

where $\eta_p(t)$ is the function describing the permanent seafloor motion. $\mathbf{T}_\tau$ is the time-shift operator where τ is the shift. Using the properties of Fourier and Laplace transforms the relationship between the solutions corresponding to the motions in equation (15) can be obtained (see Appendix C):

$$\tilde{\xi}_p(x,\omega) = \frac{1}{1 - e^{-\omega\tau}}\tilde{\xi}_e(x,\omega) \qquad (16)$$

where the tilde denotes the Laplace transformed function with respect to t, and $\xi_p(x,t)$ and $\xi_e(x,t)$ are, respectively, the solutions corresponding to permanent displacement and elastic motion. If the parameter τ is known (for instance from the seismic network), then

equation (16) can be solved and, as in the case of permanent displacement, information on the source motion can be obtained. Thus, not only more complicated sea floor motion can be constructed by starting from permanent displacement, but the results obtained above for the acoustic modulation can also be extended to the case of more complicated motion.

4.1. Limitations of the model

Attention must be paid in the interpretation of the results obtained for many different reasons. The Darcy-based model presented here, is a simplified representation of the real ocean and here we assume a flat sea bottom within a 2-D model which takes into account neither the possible interference effects due to 3-D wave generation and bathymetric gradients nor eventual signal masking due to environmental noise. Moreover, the contribution of the non-linear effects during tsunami generation is neglected [*Novikova and Ostrovsky,* 1982; *Nosov and Skachko,* 2001 and 2002 and *Nosov et al.*, 2008].

In the Darcy-based model, the compressibility in the porous layer is not taken into account. To better describe the effect of compressibility of the sedimentary porous layer on the acoustic waves this contribution has been modelled apart (see "Tokachi-Oki mismatch" sub-section below and Appendix B).

In spite of its limitations the Darcy-based model provides significant new information on tsunami generation by taking into account the porous sea bed, and shows that the acoustic signal generated by ground motion presents relevant features directly

related to the distance, extension, velocity, amplitude, frequency, and water-column height at the source.

4.2. Tokachi-Oki mismatch

In model described above we used the Darcy equation to take into account porosity and permeability effects by assuming compressibility only in the water layer. By extending the assumption of compressibility to the sedimentary layer, one can explain the mismatch, presented in the paper of *Nosov and Kolesov* [2007], between the computed and observed spectrum peaks in the Tokachi-Oki 2003 event. In a later paper *Nosov et al*, [2007], estimated a range of values for the correction of this frequency peak mismatch using a transcendent equation, to take into account the "coupled vibrations" of two non-viscous layers (characterized by height, density and the speed of sound in water and sediment respectively).

To evaluate the contribution of the sedimentary layer to the frequency spectrum of the waves generated by bed motion, it can be modelled as a homogeneous fluid-like viscous layer [*Buckingham,* 1997], with mean density ρ_s and bulk viscosity ranging from 10^6 up to 10^{20} Pa s [*Kimura,* 2006; *van Keken,* 1993]. Considering that the tsunami wavelengths are of the order of about 10÷1000 km (with typical frequencies lower than 0.01 Hz) and that the wavelength of the generated acoustic waves are thousands of meters (with frequencies ranging from 0.05 to 1Hz), then the sediment granularity, together with the effect of the small irregularities and of porosity, can be "treated as a bulk fluid in which sound propagation is governed by internal losses arising at grain-to-grain contacts" [*Buckingham,* 1997]. Assuming the above, we have developed a two-layer compressible model (see Appendix B) which, when fed with input parameters similar to those given by

Nosov and Kolesov [2007], reproduces the measured value of the frequency peak related to the water layer (see Figure 10). We correctly predict the "measured" value of 0.15Hz for the peak using a sediment thickness of 1000 m, a sediment density ρ_s = 1850 kg/m^3, and sound speed in the sediment of 2000 m. The bulk viscosity is fixed at 2*10^{10} Pa s. The other parameters are: source area semi-length a=112 km and the virtual pressure sensor (PG2 in *Nosov and Kolesov*, [2007]) was on the sea-bed at a distance x=96 km from the epicenter. The seafloor motion is a sinusoid of 8 s period and amplitude η= 1 m with no-residual displacement.

The coupling between the two compressible layers shifts some frequency peaks and produces a new peak distribution in the power spectrum, with respect to the Darcy-based model. The presence in the water column of a strong peak at 0.15 Hz (lower than the 0.1705Hz value expected from compressible models with an incompressible sedimentary layer) should be excluded by the Tolstoy cut-off [*Tolstoy,* 1963]. This gives rise to some doubts about the appropriateness of applying this cut-off in the presence of porous sediment. In conclusion, the introduction of a porous sedimentary layer may be the clue to solving the main problems arising in *Nosov and Kolesov* [2007], i.e., the overestimated amplitude of the power spectrum and the higher frequency of the water layer frequency peak.

4.3. Towards hydro-acoustic signal measurement

The measurement and characterization in real ocean situations of the hydro-acoustic signal generated by sea-bed motion is a key element for evaluating the use of these signals for warning purposes as well as for seismic studies. In this respect, the Gulf of Cadiz could become a laboratory for measuring and studying hydro-acoustic signals,

keeping in mind that tsunami early warning should be the final target. In this area a large amount of geophysical data have been collected over the past twelve years, particularly through the BIGSETS and NEAREST European projects (http://nearest.bo.ismar.cnr.it) and the SWIM ESF project. In particular, a moderate seismic activity is present and it is concentrated along a belt from the Gulf of Cadiz to the Azores [*Zitellini et al.,* 2008]. *Zitellini et al.*[2004] showed that the main tsunamigenic tectonic sources in the area are located near the coastline at about 3000 m or in shallower water , and face a deeper abyssal plain. In this particular environment, an acoustic antenna equipped with suitable low frequency hydrophones (presently under development within ESONET NoE-LIDO DEMO mission) deployed on the abyssal plain and operated jointly with 3-component bottom seismometer and bottom pressure sensor, could detect acoustic waves generated from local sources (up to hundreds of kilometers from epicenters).

An initial estimation of the hydro-acoustic environmental noise present in the area at those depths and its possible correlation with a seismic signal can be extracted from the data collected during the one-year NEAREST experiment performed in the Gulf of Cadiz, (concluded in August 2008 [*Geissler et al.,* 2009]). The acoustic waves, when detected, could be compared with seismic and bottom pressure signals acquired by the NEAREST-GEOSTAR abyssal station. A further deployment of the abyssal station in the same area is planned during 2009, together with the installation of several local land seismic stations (Portuguese, Spanish and Moroccan).

5. Conclusions

The introduction of a porous sedimentary layer in compressible models of tsunami generation can address some points, not considered by models which ignore the sediment contribution, but which are critical for a correct real measurement prediction [*Nosov and Kolesov,* 2007]. The porous sediment attenuates both the water and acoustic wave amplitudes, overestimated by compressible models, and allows for a more realistic reproduction of particular frequency features of the power spectrum, which were measured during the Tokachi-Oki 2003 event, [*Nosov and Kolesov,* 2007; *Nosov et al,* 2007]. Furthermore the porous sediment acts as a natural low pass filter for hydro-acoustic waves. Some doubts are raised about the effectiveness of the Tolstoy cut-off mechanism in the presence of porous sediments (see also *Naoi et al.,* [2006]), thus allowing the possibility of propagation of the hydro acoustic waves, upslope and at a considerable distance from the source area.

The model also shows that some remarkable characteristics can be extracted from the acoustic signal generated in the water layer by seafloor motion.

Summarizing:

1) One of the main effects of the porous layer is low-pass filtering of the signals and damping of the tsunami wave and acoustic signal amplitude: the incompressible porous layer acts as a viscous medium.

2) The coupling of a compressible porous sediment layer with the water layer produces a coupling of the modes in the hydro-acoustic signals which changes the power spectrum distribution.

3) The acoustic signal generated by the sea-floor motion, reaches the observation points much earlier than any possible tsunami wave, even in very deep water.

Starting from the model, by applying a semi-empirical analysis of the outputs from a number of simulations we found that:

4) In the acoustic signal, the number of pulses (modulation packets), the amplitude of the signal and the mean slope of the pulses scale with the source length. The acoustic signal also carries information on sea bottom velocity and water depth at the source.

5) This information can be extracted from the signal on the arrival of the very first pulses.

6) Interference between bottom motion period and the fundamental period of the water layer does not eliminate the source motion information contained in the acoustic signal;

7) The acoustic signal shows only low attenuation in amplitude even at long distances from the source.

In conclusion, the introduction of the porous sediment layer can resolve some critical issues shown by rigid bed models and, in particular, the overestimation of the power spectrum amplitude and distribution of frequency peaks. The applicability of the Tolstoy cut-off to hydro-acoustic signals is called into question in the presence of porous sediments.

In the model, the hydro-acoustic signal and its modulation carry a surprising amount of information about source parameters, sea-bed motion as well as the energy that the ground motion releases into the water column. This information, if extracted from a real hydro-acoustic signal, may allow the development of a tsunami-early warning

technique based on this acoustic "precursor". This technique could be integrated into a tsunami early warning system, and moreover might give outstanding information on the source ground motion. The application of these results to the real ocean will require a great deal of theoretical as well as experimental work.

Appendix A

This Appendix provides details on the solution of the equation of motion within the water layer and porous sediment (see equations 13 and 14). In particular, when solving equations (5) and (7), in Laplace and Fourier spaces and imposing the boundary conditions, the problem reduces to a linear system of four equations in the four functions $A(w,k)$, $B(w,k)$, $C(w,k)$, $D(w,k)$. The first two define the pressure field into the water column, while the other two define the pressure field within the porous sediment layer. Moreover, using the linear deconvolution algorithm, it is possible to reconstruct the free-surface signal starting from the pressure signal within the water layer, evaluated at a fixed depth z_0.

The functions $A(k,\omega)$ and $B(k,\omega)$, used in equation. (13), are defined as:

$$A = \frac{\omega^2}{g\alpha} B(k,\omega) \quad (17)$$

$$B = -2\mu_p(\omega)\omega \frac{\sinh(kh)}{\cosh[k(h+h_s)]} \frac{\psi(k,\omega)}{A_S(k,\omega)\sinh(\alpha h) + A_C(k,\omega)\cosh(\alpha h)} \quad (18)$$

The functions *C(k,ω)* and *D(k,ω)*, describing the pressure field within the porous domain, equation (14), can be derived from *B(k,ω)*.

$$C = -\left\{ \sinh(kh) r(k,\omega) + \frac{\alpha \mu_P}{k\cosh(kh)} \left[\cosh(\alpha h) \frac{\omega^2}{\alpha g} + \sinh(\alpha h) \right] \right\} B(k,\omega) \quad (19)$$

$$D = \cosh(kh) r(k,\omega) B(k,\omega) \quad (20)$$

The symbols used in *A(k,ω)*, *B(k,ω)*, *C(k,ω)* and *D(k,ω)* are defined as:

$$\mu_p(\omega) = \frac{\mu}{K_p} + \frac{\rho\omega}{n} \quad (21)$$

$$\alpha = \sqrt{k^2 + \frac{\omega^2}{c^2}} \quad (22)$$

$$A_S(k,\omega) = \frac{2k\rho\omega^3}{\alpha g}[1 - \cosh^2(\mathrm{kh})\mathrm{t_h}(\mathrm{k})] + \mu_p(\omega)\alpha\sinh(2\mathrm{kh})\mathrm{t_h}(\mathrm{k}) \quad (23)$$

$$A_C(k,\omega) = 2k\rho\omega[1 - \cosh^2(\mathrm{kh})\mathrm{t_h}(\mathrm{k})] + \frac{\mu_p(\omega)\omega^2}{g}\alpha\sinh(2\mathrm{kh})\mathrm{t_h}(\mathrm{k}) \quad (24)$$

$$t_h(k) = 1 - \tanh(kh)\tanh[k(h+h_S)] \quad (25)$$

$$r(k,\omega) = \rho\omega\left[\sinh(\alpha h)\frac{\omega^2}{\alpha g} + \cosh(\alpha h)\right] - \frac{\alpha\mu_P}{k}\tanh(kh)\left[\cosh(\alpha h)\frac{\omega^2}{\alpha g} + \sinh(\alpha h)\right] \quad (26)$$

$\psi(k,\omega)$ is the Laplace (time) and Fourier (x space coordinate) transform of the bottom floor motion $\eta(x,t)$:

$$\eta(x,t) = \frac{1}{2\pi i}\int_{s-i\infty}^{s+i\infty} d\omega\left[\frac{1}{2\pi}\int_{-\infty}^{+\infty} dk\,\psi(k,\omega)e^{\omega t+ikx}\right] \quad (27)$$

The permanent displacement is described by the function:

$$\eta(x,t) = \eta_0\left[\theta(x+a) - \theta(x-a)\right]\frac{\left[\theta(t)t - \theta(t-\tau)(t-\tau)\right]}{\tau} \quad (28)$$

where θ is the Heaviside function.

The pressure fluctuations at depth z can be obtained using eq. (6):

$$P(x,z,t) = -\rho\frac{1}{4\pi^2 i}\int_{s-i\infty}^{s+i\infty} d\omega \int_{-\infty}^{+\infty} dk\ \omega f_p(k,\omega,z)B(\omega,k)e^{\omega t + ikx} \quad (29)$$

where

$$f_p(k,\omega,z) = \frac{\omega^2}{\alpha g}\sinh(-\alpha z) + \cosh(-\alpha z) \quad (30)$$

The free-surface elevation, obtained using eq. (8), is similar to the previous expression for the pressure field, except for the multiplying integrand factor $f_p(k,\omega,z)$. In fact,

$$\xi(x,t) = -\frac{1}{g}\frac{1}{4\pi^2 i}\int_{s-i\infty}^{s+i\infty} d\omega \int_{-\infty}^{+\infty} dk\ \omega B(k,\omega)e^{\omega t + ikx} \quad (31)$$

Using the properties of the Laplace and Fourier transforms, the pressure field at depth, given by equation (29), can be obtained from the linear convolution between the free-surface perturbation, given by equation (31), and the inverse Laplace and Fourier transforms of the function $f_p(\omega,k,z)$. In other words, the source information carried in the free-surface modulation is still present at depth and can be recovered by applying a linear de-convolution.

Appendix B

The porous sediment is treated as a fluid-like, homogeneous and isotropic medium. The propagation of the acoustic waves is described by the wave equation with a dissipation term, represented by a sediment effective viscosity ν_s (as proposed by *Lighthill* [1993] and *Buckingham* [1998]), to take into account inter-granular friction within the sediment itself.

The porous layer is characterized by the density ρ_s and the speed of sound within it, c_s the motion being described by a velocity potential φ_s

$$U_S = \nabla \varphi_S \quad (32)$$

The motion equations for the coupled water column and the sediment viscous layer are defined as:

$$\frac{\partial^2 \varphi}{\partial t^2} = c^2 \nabla^2 \varphi \qquad (-h \le z \le 0) \quad (33)$$

in the water layer, and

$$\frac{\partial^2 \varphi_S}{\partial t^2} = \left[{c_S}^2 + 2\nu_S \frac{\partial}{\partial t} \right] \nabla^2 \varphi_S \qquad (-(h + h_S) \le z \le -h) \quad (34)$$

in the sedimentary layer.

The boundary condition at the free surface is given by

$$\frac{\partial^2 \varphi_S}{\partial t^2} = -g \frac{\partial \varphi}{\partial z} \qquad (z = 0) \quad (35)$$

whereas the boundary conditions at the water-sediment interface are:

$$\rho \frac{\partial \varphi}{\partial t} = \rho_S \frac{\partial \varphi_S}{\partial t} \qquad (z = -h) \quad (36)$$

$$\frac{\partial \varphi}{\partial z} = \frac{\partial \varphi_S}{\partial z} \qquad (z = -h) \quad (37)$$

The boundary condition at the sediment basement is:

$$\frac{\partial \varphi_S}{\partial z} = \frac{\partial \eta}{\partial t} \qquad (z = -(h + h_S)) \quad (38)$$

The solutions φ and in φ_s in the water and sediment layers are:

$$\varphi(x,z,t) = \frac{1}{4\pi^2 i} \int_{s-i\infty}^{s+i\infty} d\omega \int_{-\infty}^{+\infty} dk\, e^{\omega t - ikx} \left[A(k,\omega) \sinh(-\alpha z) + B(k,\omega) \cosh(-\alpha z) \right]$$

(39)

$$\varphi_S(x,z,t) = \frac{1}{4\pi^2 i} \int_{s-i\infty}^{s+i\infty} d\omega \int_{-\infty}^{+\infty} dk\, e^{\omega t - ikx} \left[C(k,\omega) \sinh(-\alpha_S z) + D(k,\omega) \cosh(-\alpha_S z) \right]$$

(40)

where the coefficients *A*, *B*, *C* and *D* are defined as:

$$A = \frac{\omega^2}{g\alpha} B(k,\omega) \quad (41)$$

$$B = -2\omega \frac{\sinh(\alpha_S h)}{\cosh[\alpha_S (h + h_s)]} \frac{\psi(k,\omega)}{\widetilde{A}_S(k,\omega)\sinh(\alpha h) + \widetilde{A}_C(k,\omega)\cosh(\alpha h)} \quad (42)$$

$$C = \frac{1}{\sinh(\alpha_S h)} \left\{ \frac{\rho}{\rho_S} \left[\sinh(\alpha h) \frac{\omega^2}{\alpha g} + \cosh(\alpha h) \right] - \cosh^2(\alpha_S h) r(k,\omega) \right\} B(k,\omega) \quad (43)$$

$$D = \cosh(\alpha_S h) r_S(k,\omega) B(k,\omega) \quad (44)$$

The symbols used in *A(k,ω), B*(*k* ,ω), *C*(*k* ω) and *D*(*k* ω) are defined as:

$$\alpha = \sqrt{k^2 + \frac{\omega^2}{c^2}} \quad ; \quad \alpha_S = \sqrt{k^2 + \frac{\omega^2}{c_S^{\,2}}} \quad (45)$$

$$\widetilde{A}_S(k,\omega) = \frac{2\alpha_S \rho\omega^2}{\alpha\rho_S g}[1 - \cosh^2(\alpha_S h)\mathrm{t_h}(\alpha_S)] + \alpha\sinh(2\alpha_S h)\mathrm{t_h}(\alpha_S) \quad (46)$$

$$\widetilde{A}_C(k,\omega) = 2\alpha_S \frac{\rho}{\rho_S}[1 - \cosh^2(\alpha_S h)\mathrm{t_h}(\alpha_S)] + \frac{\omega^2}{g}\sinh(2\alpha_S h)\mathrm{t_h}(\alpha_S) \quad (47)$$

$$t_h(\alpha_S) = 1 - \tanh(\alpha_S h)\tanh\left[\alpha_S(h + h_S)\right] \quad (48)$$

$$r_S(k,\omega) = \left[\frac{\rho\omega^2}{\rho_S\alpha g} + \frac{\alpha}{\alpha_S}\tanh(\alpha_S h)\right]\sinh(\alpha h) + \left[\frac{\rho}{\rho_S} + \frac{\omega^2}{\alpha_S g}\right]\cosh(\alpha h) \quad (49)$$

Appendix C

In the case of seafloor motion with final permanent displacement, the free-surface solution, evaluated at fixed location x, carries significant information concerning the source motion and geometry. Different and more complicated sea-bottom motion can be obtained by combining the permanent displacements with time-shift operators (see Figure 1). The three different motions can be used in turn for the construction of more complicated seafloor motions.

The free-surface solution, corresponding to these different motions, can be related to the solution obtained for the permanent displacement, and can be inverted using the Laplace transform and its properties. As a consequence, also in the case of more complicated seafloor motions, the acoustic modulation still carries the same information about source motion and geometry.

The simple elastic seafloor motion (rise and fall) $\eta_e(t)$ given in equation (15) is obtained using the time-shift operator $\mathbf{T}_\tau$ defined as:

$$\mathbf{T}_\tau f(t) = f(t-\tau) \qquad (50):$$

From equation (18) and (31) the free-surface solution at fixed observing point x is:

$$\xi(x,t) = (\mathbf{FL})^{-1} I(k,\omega)(\mathbf{FL})\eta(x,t) = \mathbf{H}\,\eta(x,t) \quad (51)$$

where

$$I(k,\omega) = -\frac{\omega}{g}\frac{B(k,\omega)}{\psi(k,\omega)} \quad (52)$$

Here **F** and **L** are the operators corresponding to direct Fourier and Laplace transform, $B(k,\omega)$ is the coefficient shown in equation (13) and given in equation (18) and $\psi(k,\omega)$ is the direct Laplace and Fourier transform of the seafloor motion which, in the case of permanent displacement, is given by equation (28), g is the gravitational acceleration. Using the properties of the Laplace transform, with some algebra, we can show that the two operators **H** and $\mathbf{T}_\tau$ commute:

$$\mathbf{H}\mathbf{T}_\tau\eta(x,t) = \mathbf{H}\eta(x,t-\tau) = (\mathbf{FL})^{-1} I(k,\omega)e^{-\omega\tau}(\mathbf{FL})\eta(x,t) = \xi(x,t-\tau) = \mathbf{T}_\tau\mathbf{H}\eta(x,t) \quad (53)$$

Using this property, the free-surface solution ξ_e corresponding to the elastic seafloor motion described in equation (15), can be written as a function of the solution ξ_p which corresponds to the permanent displacement:

$$\xi_e = \mathbf{H}\eta_e = \mathbf{H}(1-\mathbf{T}_\tau)\eta_p = (1-\mathbf{T}_\tau)\mathbf{H}\eta_p = (1-\mathbf{T}_\tau)\xi_p \quad (54)$$

The same conclusion can be easily extended to more complicated bottom motion, due to linearity.

Equation (54) can be inverted using a Laplace transform to obtain equation (16): once the parameter τ is known, then this equation can be solved and the information on the source motion retrieved.

Acknowledgements This work was supported by the Commission of the European Communities under contract 037110 - GOCE (NEAREST Project). Particular thanks are due to Dr. Paolo Favali, Dr. Stephen Monna, Dr. Marco Ligi and Dr. Carlo Lari for many helpful discussions.

References

Baptista, M., J. Miranda, F. Chierici, and N. Zitellini (2003), New study of the 1755 earthquake source based on multi-channel seismic survey data and tsunami modelling, *Natural Hazards and Earth System Sciences, 3*, 333-340.

Bernard, E.N., and A.R. Robinson (eds.) (2009) Tsunamis. The Sea, Volume 15, Harvard University Press, Cambridge, MA and London, England

Biot M.A. (1962), Mechanics of Deformation and Acoustic Propagation in Porous Media, *J. Appl. Phys.*, *33,* 1482

Boschi, E., E. Guidoboni, G. Ferrari, G. Valensise, and P. Gasperini (Eds.) (1997), *Catalogue of the strong earthquakes in Italy from 461 BC to 1990*, 973 pp., ING & SGA, Bologna.

Buckingham M.J. (1998),Theory of compressional and shear waves in fluidlike marine sediments, *Jl Acou. Soc. Am., 103 (1)*, 288-299

Comer, R. (1984), The tsunami mode of a at earth and its excitation by earthquakesources, *Geophys. J. R. Astr. Soc., 77*, 1-27

Dutykh D., F. Dias, and Y. Kervella (2006) Linear theory of wave generation by a moving bottom, C. R. Acad. Sci. Paris, *Ser. I 343*, 499-504

Geissler W.H., L.M. Matias, S. Monna, D. Stich, A. Iben Brahim, F. Mancilla, N. Zitellini, and NEAREST Working Group, From Tides to Whale calls - Broadband ocean-bottom recordings from the Gulf of Cadiz, presented at European Geosciences Union General Assembly, Wien 19-24 April 2009

Gisler, G. (2008*),* Tsunami simulations, *Annual Review of Fluid Mechanics*, *40*, 71-90

Gu, Z., and H. Wang (1991), Gravity waves over porous bottoms, *Coastal Engineering*,*15*, 497{524.

Habel, F., and C. Bagtzoglou (2005), Wave induced flow and transport in sediment beds, *Journal of the American Water Resources Association*, *41(2)*, 461-476.

Kajiura, K. (1970), Tsunami source, energy and the directivity of wave radiation, *Bull. Earthq. Res. Inst. Tokyo Univ., 48*, 835-869.

Kimura M. (2006), Shear Wave Velocity in Marine Sediment, *Jpn. J. Appl. Phys., 45(5B),* 4824-4828

Kowalik, Z., W. Knight, T. Logan, and P. Whitmore (2005), Numerical modeling of the global tsunami: Indonesian tsunami of 26 december 2004*, Sci. Tsunami Hazard, 23(1),*40-56.

Lamb (1932), *Hydrodynamics*, Dover Pubblications, New York

Lighthill J. (1993), *Waves in Fluids*, Cambridge University Press, Cambridge, London, New York, Melbourne

Lomnitz, C., and S. Nilsen-Hofseth (2005), The indian ocean disaster: Tsunami physics and early warning dilemmas, *EOS Trans. AGU, 86*, 65-70.

Ma, K., H. Kanamori, and K. Satake (1997), Mechanism of the 1975 Kalapana, Hawaii earthquake inferred from tsunami data, *J. Geophys. Res., 104*, 13153-13167.

Merrifield, M., Y. L. Firing; T. Aarup, W. Agricole, G. Brundrit, D. Chang-Seng, R. Farre, B. Kilonsky, W. Knight, L. Kong, Magori, C., P. Manurung,C. McCreery, W. Mitchell, S. Pillay, F. Schindele, F. Shillington, L Testut, E. M. S. Wijeratne, P. Caldwell, J. Jardin, S. Nakahara, F. Y. Porter, N. Turetsky (2005), Tide gauge observations of the indian ocean tsunami, december 26, 2004, *Geophys. Res. Lett., 32*, L09,603.

Miyoshi, H. (1954), Generation of the tsunami in compressible water (Part I), *J. Oceanogr. Soc. Japan, 10*, 1-9.

NEAREST project web site: http://nearest.bo.ismar.cnr.it/.

NGDC Tsunami Catalog web site: http://www.ngdc.noaa.gov/hazard/tsu db.shtml.

Naoi, J., I. Ryoichi, K. Toshiaki and M. Koichi (2006) Variation in Cutof Effect and Sound Field Caused by Geometrical Structures near the Coast, *Japanese Journal of Applied Physics, 22 (5)*, 693-697

Novikova, L. E. and L. A. Ostrovsky, (1982), On an acoustic mechanism of tsunami wave generation*, Oceanology, 22 (5)*, 693-697

Nosov, M. A. (1999), Tsunami generation in compressible ocean, *Phys. Chem. Earth (B), 24 (5)*, 437-441.

Nosov M.A. (2000), On the tsunami Generation in the Compressible Ocean by Vertical Bottom Displacements, *Izvestiya, Atmospheric and Oceanic Physics 36 (5),* 718-726.

Nosov M.A. and K. Sammer (1998), Tsunami Excitation by a Moving Bottom Displacement in Compressible Water, *Moscow University Physics Bulletin 53 (6)*, 67-70.

Nosov, M. A., and S. N. Skachko (2001), Nonlinear tsunami generation mechanism, *Nat. Hazards Earth Syst. Sci., 1,* 251-253.

Nosov, M. A., and S. N. Skachko (2002), Nonlinear mechanism of tsunami generation in a compressible ocean, in *Local Tsunami Warning and Mitigation*, edited by B. W. Levin and M. A. Nosov, pp. 107-114, Janus, Moscow.

Nosov, M. A., and S. V. Kolesov (2007), Elastic oscillations of water column in the 2003 tokachi-oki tsunami source: in-situ measurements and 3-D numerical modelling, *Nat. Hazards Earth Syst. Sci., 7*, 243-249.

Nosov M. A., S. V. Kolesov, and A.V. Denisova (2008), Contribution of nonlinearity in tsunami generated by submarine earthquake, *Advances in Geosciences, 14*, 141-146

Nosov, M., S. Kolesov, A. Denisova, A. Alekseev, and B. Levin (2007), On the near-bottom pressure variations in the region of the 2003 Tokachi-Oki tsunami source, *Oceanology*, pp. 26-32.

Ohmachi, T., H. Tsukiyama, and H. Matsumoto (2001), Simulation of tsunami induced by dynamic displacement of seabed due to seismic faulting, *Bull. Seism. Soc. Am., 91 (6),* 1898-1909.

Okada, Y. (1985), Surface deformation due to shear and tensile faults in a halfspace, *Bull. Seismol. Soc. Amer.*, *75*, 1135–1154.

Okal, E. A. (1988), Seismic parameters controlling far-field tsunami amplitudes: a review, *Natural Hazards, 1*, 67-96.

Okal, E. A., P.J. Alasset and O. Hyvernaud, F. Schindele (2003), The deficient T waves of tsunami earthquakes, *Geophys. J. Int.l, 152 (2)*, 416-432.

Panza, G., F. Romanelli, and T. Yanovskaya (2000), Synthetic tsunami mareograms for realistic oceanic models, *Geophys. J. Int.l, 141*, 498-508.

Sells, C. C. L. (1965), The effect of a sudden change of shape of the bottom of a slightly compressed ocean, *Phil. Trans. R. Soc. London (A), 258*, 495-528.

Synolakis, C. (1995), Tsunami prediction, *Science*, *270,* 15-16.

Synolakis, C., P. Liu, G. Carrier, and H. Yeh (1997), Tsunamigenic seafloor deformation, *Science, 278*, 598-600.

Synolakis, C., J. Bardet, J. Borrero, H. Davies, E. Okal, E. Silver, J. Sweet, and D. Tappin (2002), Slump origin of the 1998 Papua New Guinea tsunami, *Proceedings of the Royal Society of London A, 458*, 763-769.

Tolstoy, I. (1963), The theory of waves in stratified uids including the effects of gravity and rotation. *Rev. Mod. Phys., 35*, 207230.

Tinti, S., A. Maramai, and L. Graziani (2004), The new catalogue of italian tsunamis, *Natural Hazards, 33*, 439-465.

van Keken P.E., C.J. Spiers, A.P. van den Berg, and E.J. Muyzert (1993), The effective viscosity of rocksalt: implementation of steady state creep laws in numerical models of salt diapirism, *Tectonophysics, 225*, 457-476

Ward, S. (1980), Relationships of tsunami generation and an earthquake source, *J. Phys. Earth, 28*, 441-474.

Ward, S. (1981), On tsunami nucleation: I. a point source, *J. Geophys. Res., 86*, 7895-7900.

Ward, S. (1982), *On* tsunami nucleation: II. an instantaneous modulated line source, *Phys. Earth Planet. Inter., 27*, 273-285.

Zitellini, N., F. Chierici, R. Sartori, and L. Torelli (1999), *The* tectonic source of the 1755 Lisbon earthquake and tsunami, *Annali di Geofisica, 42*, 49-55.

Zitellini N., E. Gràcia, L. Matias, P. Terrinha, M.A. Abreu, G. DeAlteriis, J.P. Henriet, J.J. Dañobeitia, D.G. Masson, T. Mulder, R. Ramella, L. Somoza and S. Diez , *The quest for the Africa–Eurasia plate boundary west of the Strait of Gibraltar,* in press to Earth Planet. Sci. Lett.

Figure 1. Different kinds of motion are shown: on the left the time history and on the right the corresponding piston-like motions. The first row represents the basic permanent displacement from which more complicated motion can be obtained.

Figure 2. (a) a comparison at fixed time of a tsunami profile in the generation area with a porous layer against a non-permeable layer. Green dotted lines delimit the bottom motion area. The tsunami generation is captured at about 100s from the initial bottom motion. Motion duration is τ=20s and the length a=5km. (b) a comparison between porous (black line) and non-permeable bed (red line) is shown at x=75km from the source

and for a bottom motion duration of τ=3s and a displacement semi-length a=10km. Sediment thickness is h_s= 2500m and water depth is h= 1500m. Porosity n=0.5 and permeability is $K_p=10^{-6}$ cm^2. The effect of the porosity is a lowering of the acoustic modulation and tsunami amplitude, and a frequency smoothing. (c) shows the power spectrum, corresponding to (a), (d) is a zoom of (c) (linear amplitude). The frequency cut-off due to the action of porosity is clearly visible.

Figure 3. Free-surface plots at: (a) x=100km, (b) x=300km from the source. The parameters of the simulation are η_0=1m for the bottom displacement and τ =25s the duration of the motion. The displacement length is chosen at 2a= 60km in a h=3000m water depth. The porous seabed thickness is h_s=1500m, volumetric porosity n=0.3 and permeability $K_p=10^{-6}$ cm^2. The acoustic modulation and tsunami are shown; the inset in box (b) is a zoom of the first part of the acoustic modulation. Boxes (c) and (d) show the pressure signal corresponding to (a) and (b), but at z=1500m water depth.

Figure 4. The observing distance is chosen at x=300km and the water layer is h=1500m deep. The sedimentary bed has a thickness of h_s=750m for a τ=1s motion duration. Bottom motion amplitude, and permeability and porosity are the same as in Figure 3. The acoustic modulation, due to different source semi-lengths of a=15km, and a=45km is shown in boxes (a) and (b). As can be clearly noted in the zoomed envelopes of boxes (c) and (d), the number of pulses in the same time interval varies with source length, scaling with the ratio among these lengths.

Figure 5. The semi-length of the source is chosen as a=15km. The point of observation is located at a distance x=300km from the source and all the other parameters are the same as in Figure 4. The boxes (a), (b) and (c) show the acoustic modulation, with the envelopes superimposed, for different source velocities v=η_0/τ (in boxes (a) v=1m/s, (b), v=0.2m/s, (c) v=0.1m/s). Box (d) shows a comparison between envelopes, with the values of the mean slopes of the associated pulses (shown by arrows). The mean slope variation is directly proportional to the velocity variation. As in Figure 4, the mean slope is an indicator of the energy released into the water by the ground motion, but the number of pulses is the same within the same time interval.

Figure 6. The envelopes of permanent displacement motions with periods τ=4s , τ=8s (a), τ=12s and τ=16s (b) are shown in boxes (a), (b) and (c). In this simulation a h=1500m water depth is chosen, a sediment thickness of h_s=750m, a source semi-length of a=15km and the observation point is located at x=375km from the source. All other parameters are the same as in Figure 4**.** The interference between the seafloor motion frequency and the fundamental water-layer frequency of oscillation leads to a very different modulation pattern with respect to that caused by the same seafloor motion but with frequencies far from the fundamental water-layer frequency. Moreover, the modulation amplitude is an order of magnitude smaller. As can be seen in box (c), the different "interference" periods produce similar envelopes, which in the first pulses scale in amplitude with bottom velocities (or equivalently with the periods as the motion is the

same for each simulation) and then flatten into tails of equal amplitudes before the tsunami arrives (about 3091s in this simulation). Box (d) shows the distribution of the mean slopes plotted against the "interference" bottom motion periods of τ=4s, 8s, 12s, 16s, 20s, 24s, 28s and 32s. The linear trend is clearly recognizable, with a correlation coefficient of r^2 =0.9987.

Figure 7. An example of a tsunami generated by a permanent displacement bottom motion with 24s "interference" period. The observation point is 100km from the source. All other parameters are the same as in Figure 3(a): the resulting tsunami amplitude is also the same as in Figure 3a. On the contrary the amplitude of the hydro-acoustic signal is smaller.

Figure 8. The power spectrum corresponding to Figure 6(a) , "interference" bottom motion period of 8s, shown in box (a). Box (b) shows the power spectrum obtained for a period of 10s, all other parameters of the simulation being the same.

Figure 9. The hydro-acoustic signal produced by a source with a length shorter than the water depth. Modulation of the acoustic signal is not present. Here the source semi-length is a=1km, the water depth is 4500m and the observing point is chosen at 100km from the source. The motion causes a permanent displacement over a 3s period.

Figure 10. Comparison between the power spectra of a two-layer compressible sediment model in light grey (Appendix C) and an incompressible porous sediment model in black (Darcy model).The measured value of 0.15hz for the frequency peak is correctly predicted by the compressible model for a choice of parameters compatible and similar to those given for the PG2 pressure gauge by *Nosov and Kolesov* [2007]. We use a sediment thickness of 1000m, a sediment density ρ_s = 1850kg/m^3 and a speed of sound in the sediment of 2000m/s. The bulk viscosity is fixed at $2*10^{10}$ Pa*s. The other parameters are a source area semi-length a=112km and the virtual pressure sensor placed on the sea-bed at a distance x=96km from the epicenter. The seafloor motion is a sinusoid of 8s period and amplitude η= 1m with no residual permanent displacement. The different frequency peak distribution is due to the coupling between the two compressible layers.

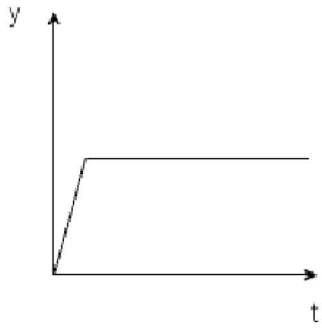
y
t

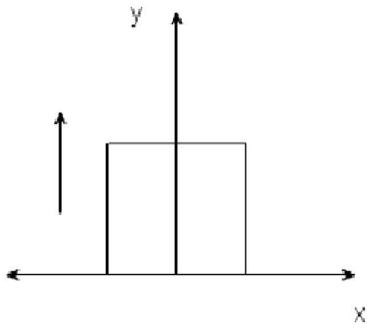
y
x

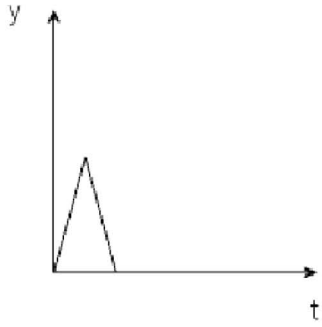
y
t

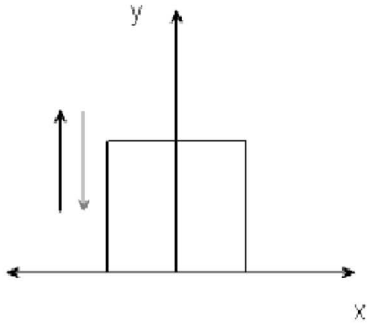
y
x

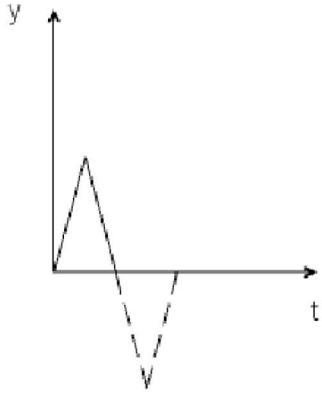
y
t

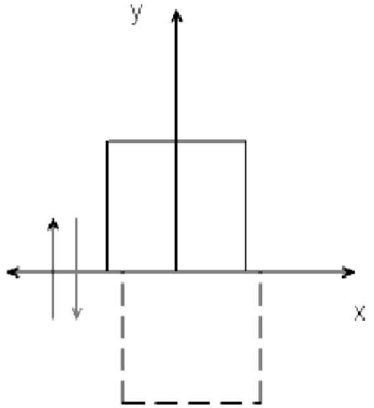
y
x

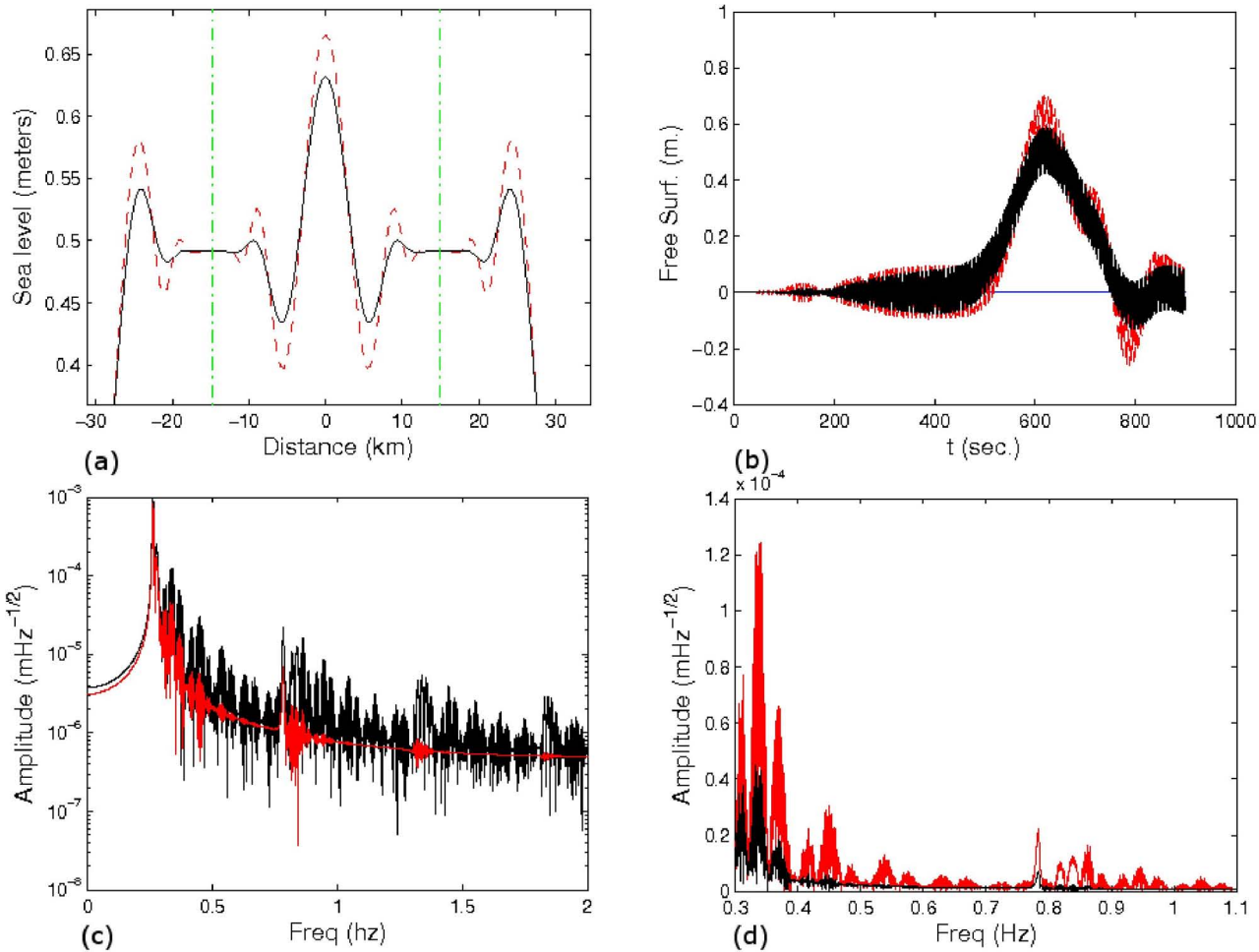
Sea level (meters)
Distance (km)
(a)
Free Surf. (m.)
t (sec.)
(b)
Amplitude (mHz$^{-1/2}$)
Freq (hz)
(c)
x 10^{-4}
Amplitude (mHz$^{-1/2}$)
Freq (Hz)
(d)

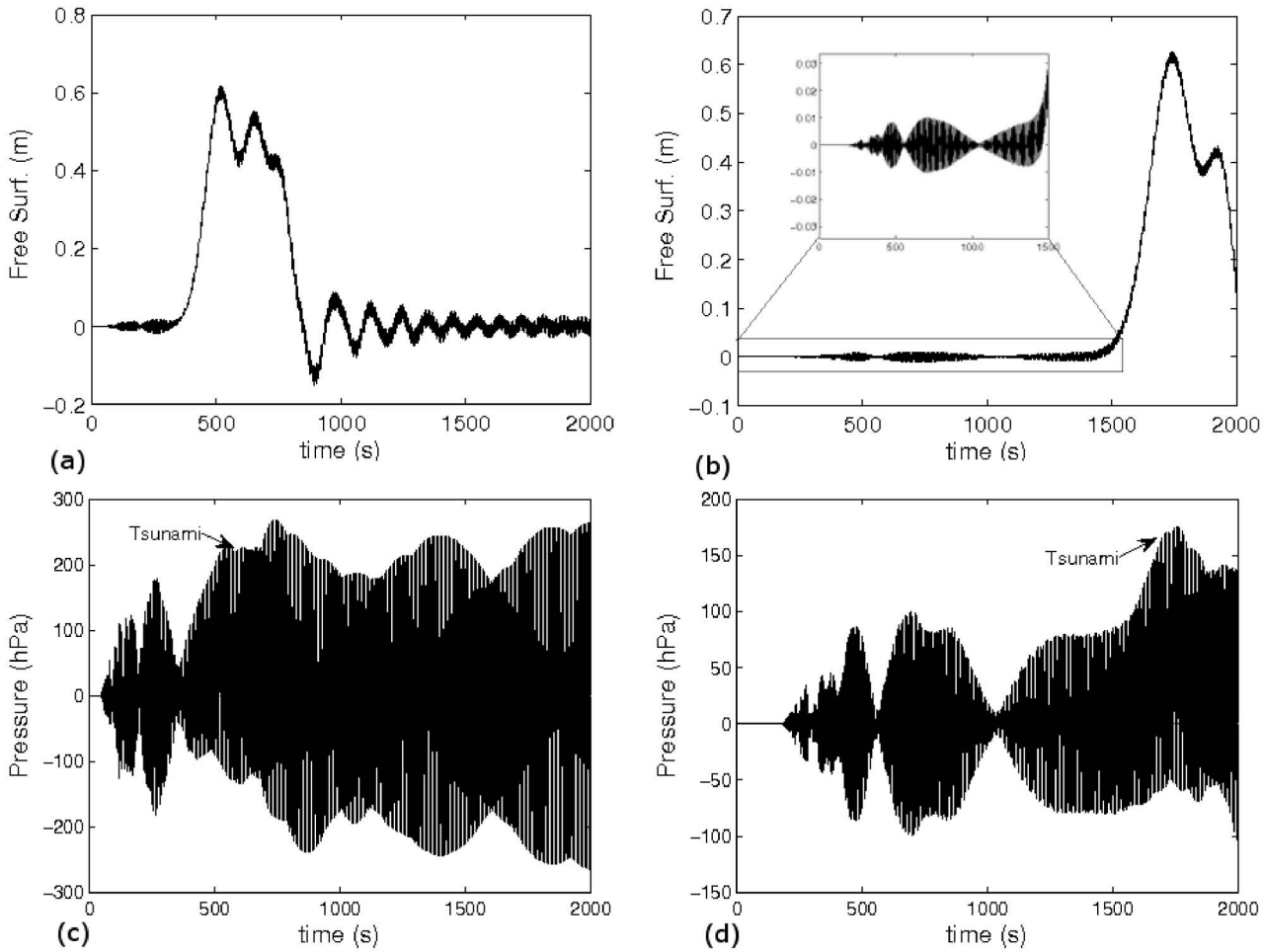
Free Surf. (m)
time (s)
(a)
Free Surf. (m)
time (s)
(b)
Tsunami
Pressure (hPa)
time (s)
(c)
Tsunami
Pressure (hPa)
time (s)
(d)

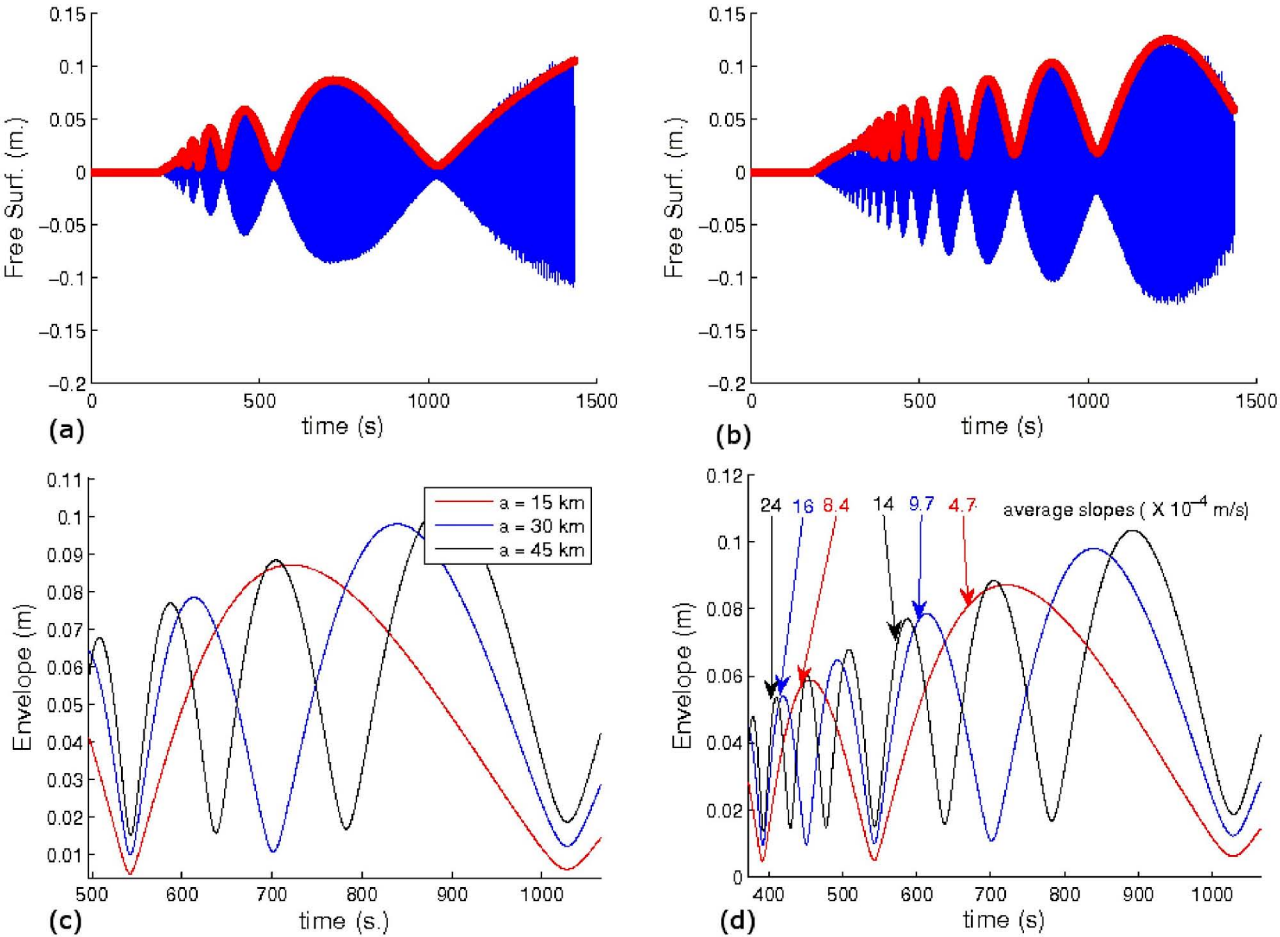
Free Surf. (m.)
time (s)
(a)
(b)
Envelope (m)
time (s.)
(c)
a = 15 km
a = 30 km
a = 45 km
24
16
8.4
14
9.7
4.7
average slopes (X 10^{-4} m/s)
time (s)
(d)

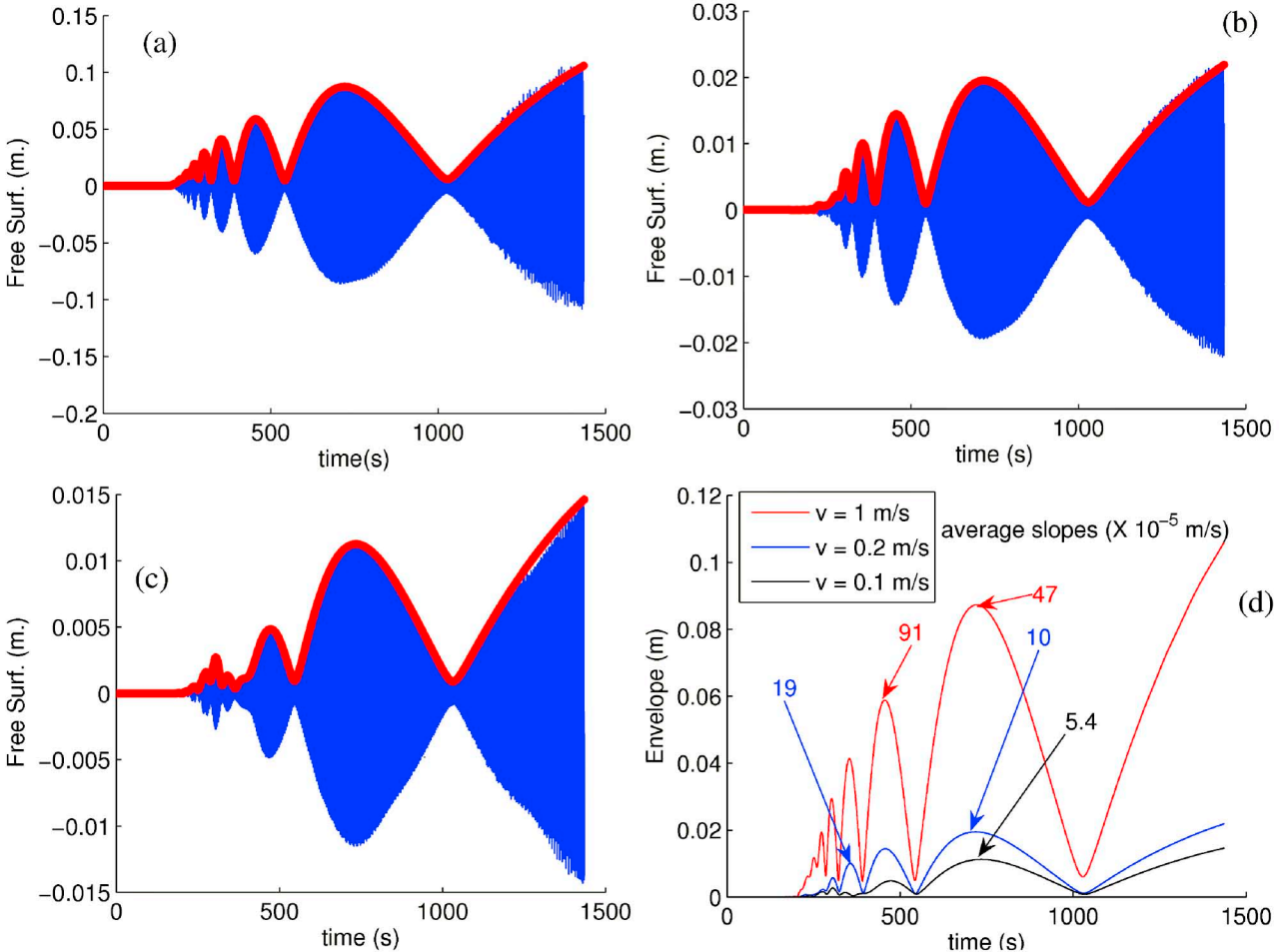
(a)
Free Surf. (m.)
time(s)
(b)
Free Surf. (m.)
time (s)
(c)
Free Surf. (m.)
time (s)
(d)
v = 1 m/s
v = 0.2 m/s
v = 0.1 m/s
average slopes (X 10^-5 m/s)
47
91
10
19
5.4
Envelope (m)
time (s)

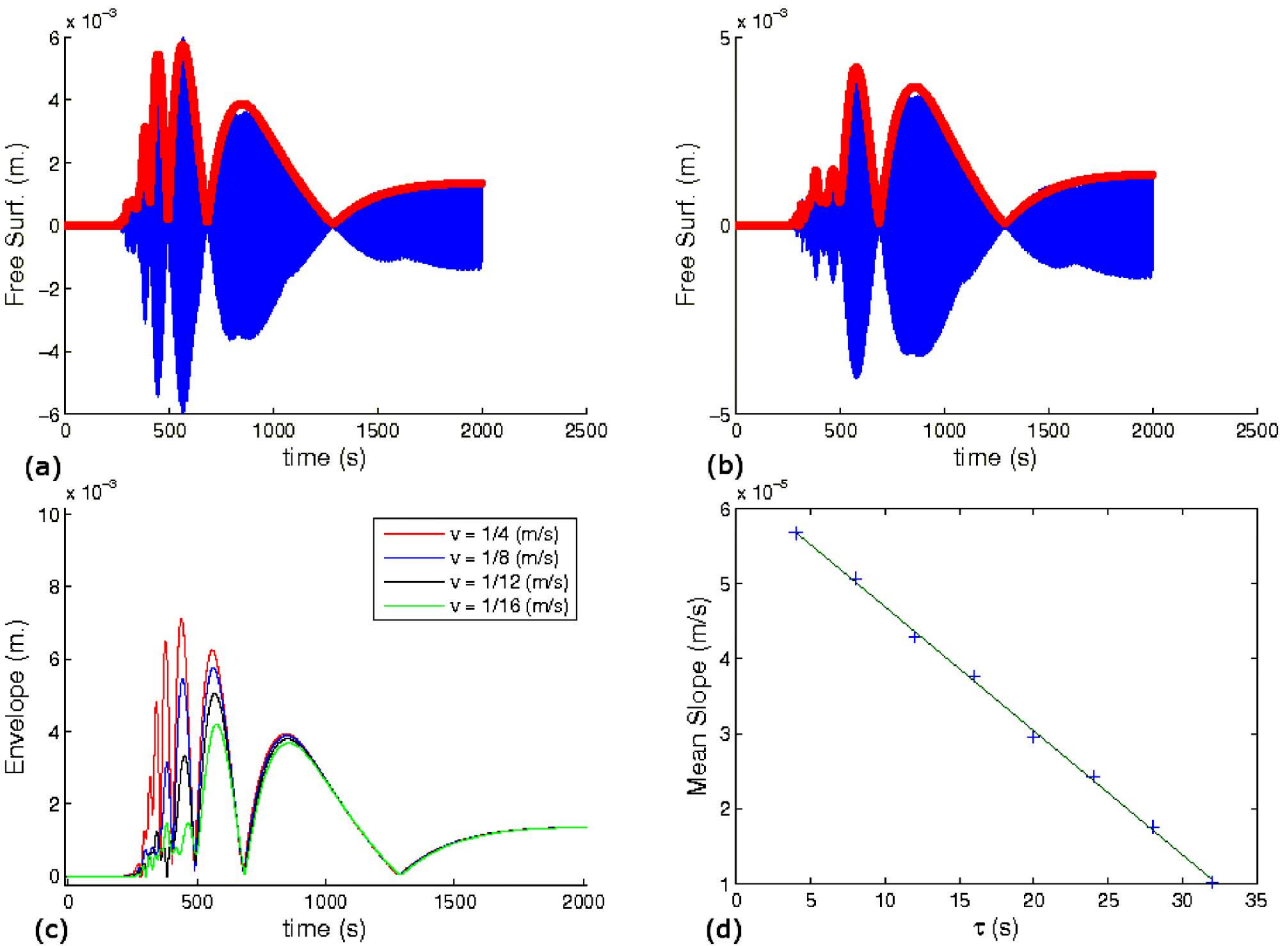
x 10^-3
Free Surf. (m.)
time (s)
(a)
x 10^-3
Free Surf. (m.)
time (s)
(b)
x 10^-3
Envelope (m.)
v = 1/4 (m/s)
v = 1/8 (m/s)
v = 1/12 (m/s)
v = 1/16 (m/s)
time (s)
(c)
x 10^-5
Mean Slope (m/s)
τ (s)
(d)

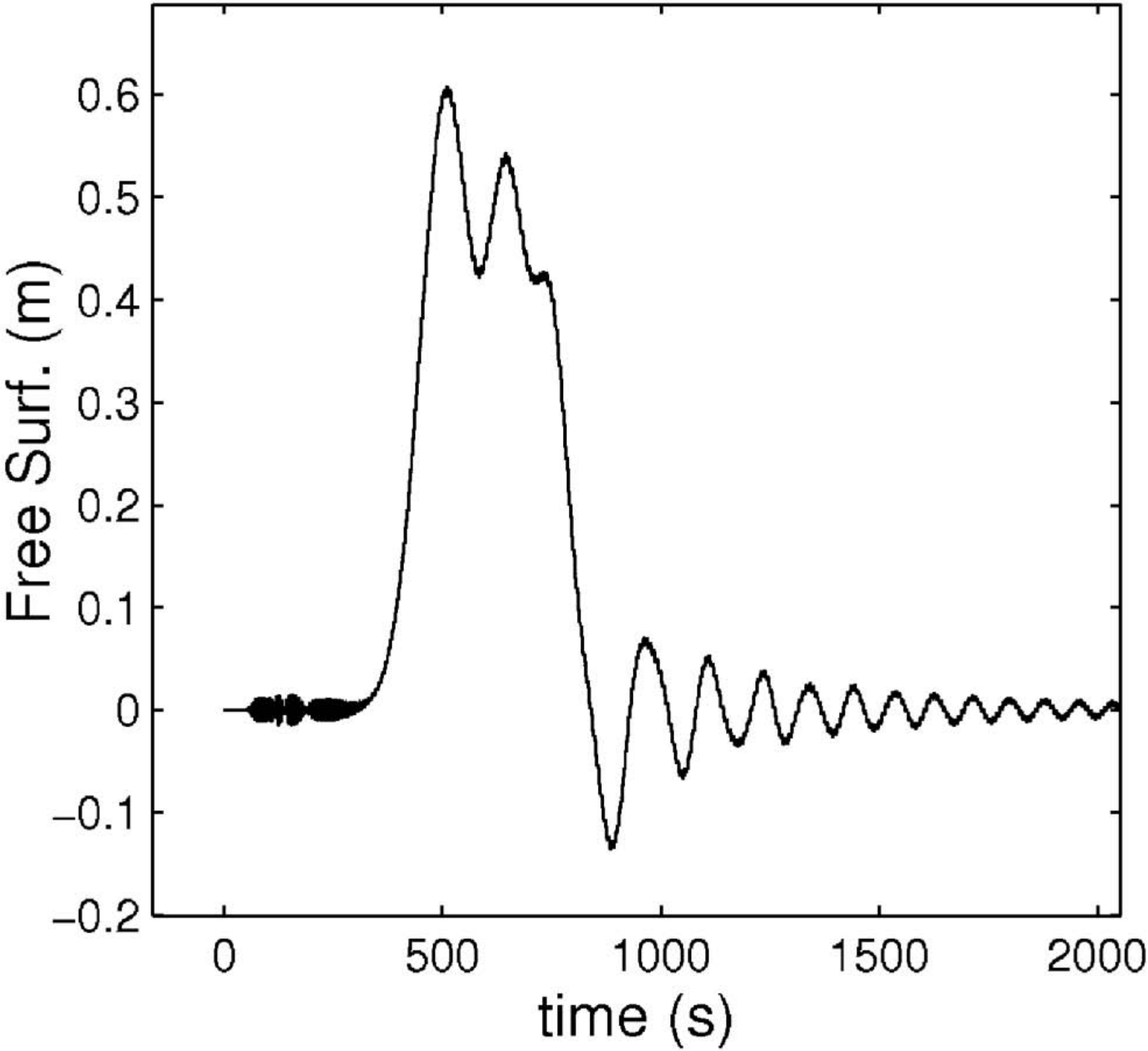
0.6
0.5
0.4
0.3
0.2
0.1
0
−0.1
−0.2
Free Surf. (m)
0
500
1000
1500
2000
time (s)

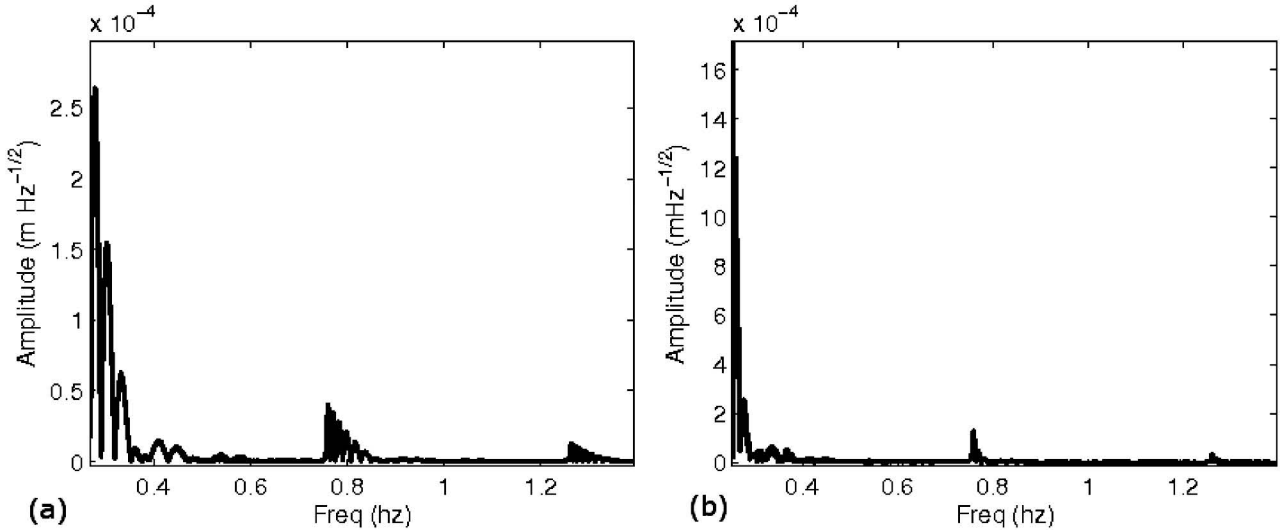
x 10^-4
Amplitude (m Hz^-1/2)
2.5
2
1.5
1
0.5
0
0.4
0.6
0.8
1
1.2
Freq (hz)
(a)
x 10^-4
Amplitude (mHz^-1/2)
16
14
12
10
8
6
4
2
0
0.4
0.6
0.8
1
1.2
Freq (hz)
(b)

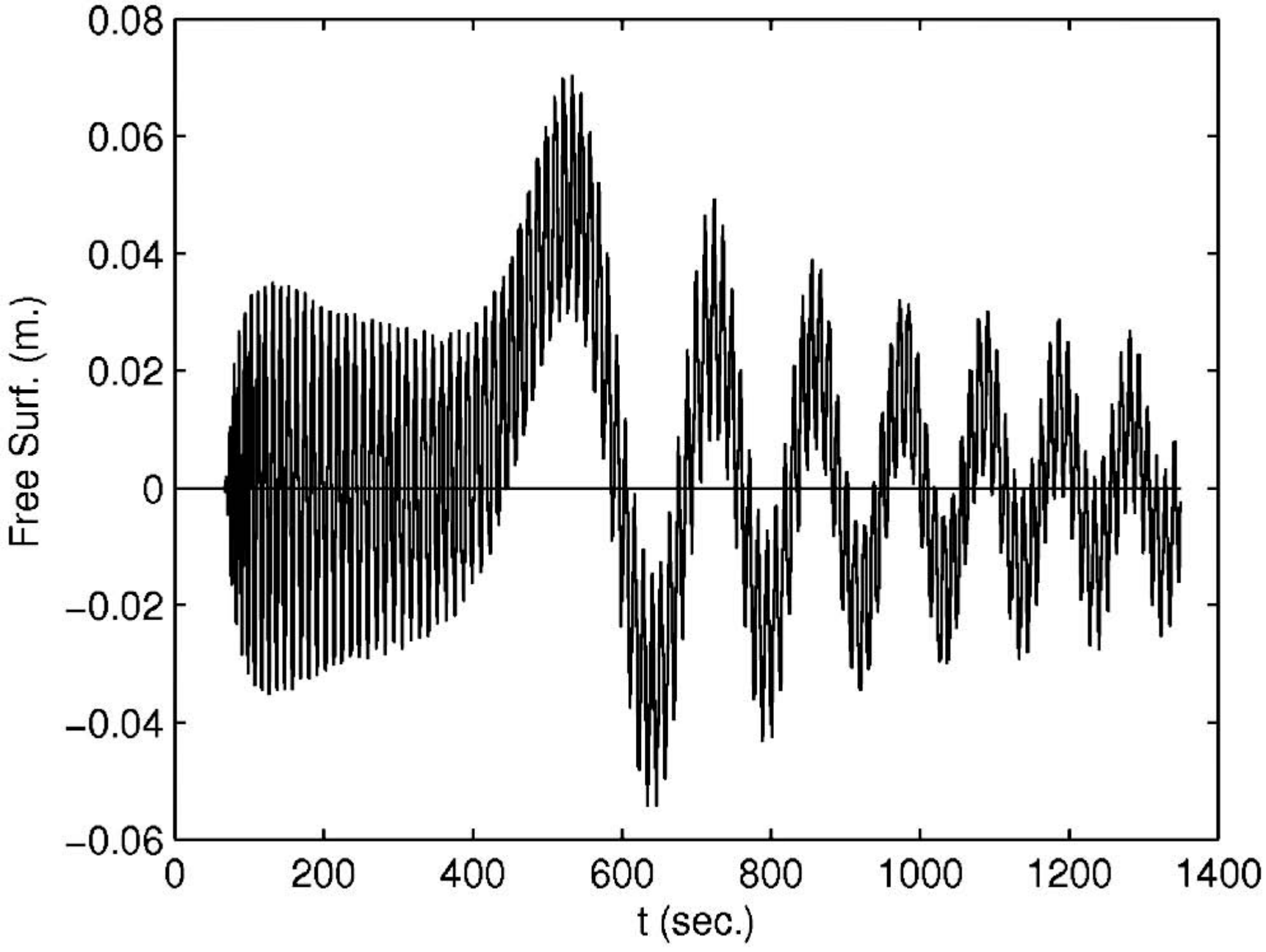
0.08
0.06
0.04
0.02
0
−0.02
−0.04
−0.06
Free Surf. (m.)
0
200
400
600
800
1000
1200
1400
t (sec.)

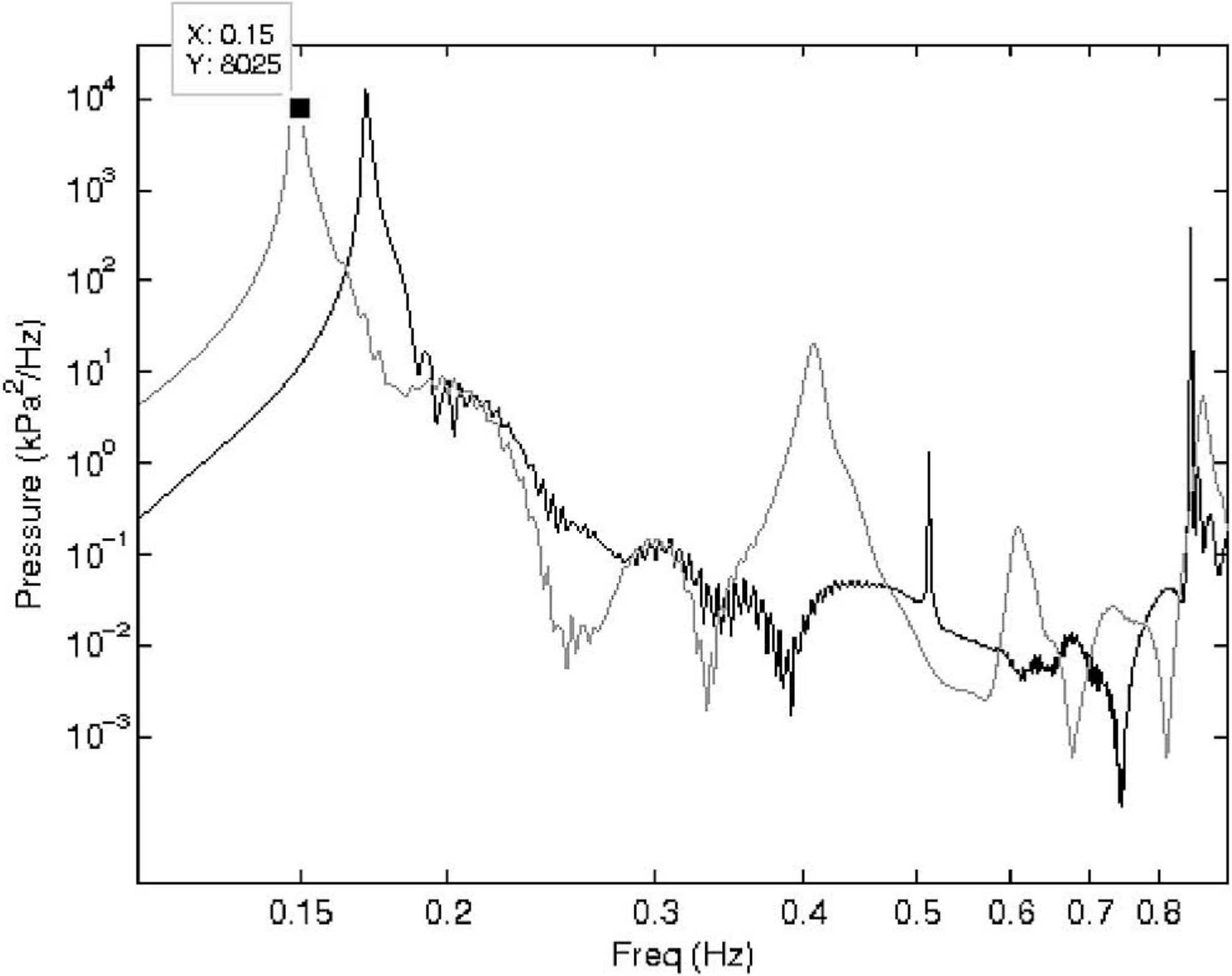
X: 0.15
Y: 8025
Pressure (kPa²/Hz)
10⁴
10³
10²
10¹
10⁰
10⁻¹
10⁻²
10⁻³
0.15
0.2
0.3
0.4
0.5
0.6
0.7
0.8
Freq (Hz)